

Radio-optical alignments in a low radio luminosity sample

Mark Lacy¹, Susan E. Ridgway¹, Margrethe Wold², Per B. Lilje³ & Steve Rawlings¹

¹ *Astrophysics, Department of Physics, Keble Road, Oxford, OX1 3RH, U.K.*

² *Stockholm Observatory, S-133 36 Saltsjöbaden, Sweden*

³ *Institute of Theoretical Astrophysics, University of Oslo, P.O. Box 1029 Blindern, N-0315 Oslo, Norway*

ABSTRACT

We present an optically-based study of the alignment between the radio axes and the optical major axes of eight $z \sim 0.7$ radio galaxies in a 7C sample. The radio galaxies in this sample are ≈ 20 -times less radio luminous than 3C galaxies at the same redshift, and are significantly less radio-luminous than any other well-defined samples studied to date. Using Nordic Optical Telescope images taken in good seeing conditions at rest-frame wavelengths just longward of the 4000Å break, we find a statistically significant alignment effect in the 7C sample. Furthermore, in two cases where the aligned components are well separated from the host we have been able to confirm spectroscopically that they are indeed at the same redshift as the radio galaxy. However, a quantitative analysis of the alignment in this sample and in a corresponding 3C sample from HST archival data indicates that the percentage of aligned flux may be lower and of smaller spatial scale in the 7C sample. Our study suggests that alignments on the 50-kpc scale are probably closely related to the radio luminosity, whereas those on the 15 kpc scale are not. We discuss these results in the context of popular models for the alignment effect.

Key words: galaxies: active – radio continuum: galaxies – galaxies: evolution

1 INTRODUCTION

Studies of samples of high radio luminosity radio galaxies at $z \geq 0.6$ show that the position angles of the optical and emission-line morphologies tend to align with the radio axis (McCarthy et al. 1987, Chambers et al. 1987). High-resolution optical imaging with the Hubble Space Telescope (HST) reveals that the aligned material is morphologically distributed in a wide variety of ways (e.g. Best et al. 1996, 1997b), and is unlikely to be the result of a single mechanism. With the exceptions of 3C171 (Clark et al. 1998) and 3C368 (Dickson et al. 1995; Stockton, Ridgway & Kellogg 1996), nebular continuum fails to explain more than a fraction of the aligned light in objects for which deep spectroscopy has been obtained. Scattering of a hidden quasar nucleus is expected to add to the aligned light, and the detection of broad, polarised MgII emission in a number of these objects (e.g. 3C265 and 3C324; Dey & Spinrad 1996; Cimatti et al. 1996) shows that this can be an important contributor. The closely aligned morphologies seen in the WFPC2 imaging are, however, inconsistent with pure scattering models, and star formation induced by the passage of the radio jet has been proposed by many

(e.g. Chambers et al. 1990, Best et al. 1996, Dey et al. 1997).

Most proposed mechanisms for producing radio – optical alignments are expected to depend to some extent on the AGN luminosity. The radio luminosity and the strength of narrow optical emission lines in radio galaxies have been known to correlate for some time (Baum & Heckman 1989; Rawlings et al. 1989). Recently, a correlation of the optical continuum luminosity of steep-spectrum radio-loud quasars with radio luminosity has also been established (Serjeant et al. 1998). Both these imply a close relationship between the optical/UV luminosity of the AGN and the radio luminosity, presumably via a correlation with the bulk kinetic power of the radio jets (Rawlings & Saunders 1991). Given this, it is not surprising that the optical emission aligned with the radio jet seen in high redshift radio galaxies might also correlate with radio luminosity. Two studies in the near-infrared, that of Dunlop & Peacock (1993) and of Eales et al. (1997) found that this “alignment effect” was unmeasurably small in samples of $z \sim 1$ radio sources approximately ten and four times fainter than 3C respectively. Both these studies were, however, carried out under conditions of poor ($\gtrsim 1''$)

seeing, and in the K -band (roughly 1-micron in the rest-frame), where the alignment effect is weak even in 3C (Rigler et al. 1992). They therefore could not usefully constrain how strongly the alignment effect depended on radio luminosity.

The question of the luminosity dependence of the alignment effect is also related to the extent to which the onset of the alignment effect at $z \sim 0.6$ in flux-limited samples such as 3C is a true evolutionary effect, or just an effect due to sources in a flux-limited sample becoming more luminous with redshift.

In this paper, we present optical images of a sample of $z \sim 0.7$ radio galaxies whose radio luminosity is approximately twenty times lower than those of 3C radio galaxies at the same redshift. Using these images and data on a comparison sample of 3C objects obtained from the HST archive, we quantify and compare the strength of the alignment effect in the two samples. We assume an $H_0 = 50 \text{ km s}^{-1} \text{ Mpc}^{-1}$, $q_0 = 0.5$ cosmology throughout.

2 OBSERVATIONS AND DATA REDUCTION

2.1 Imaging

Images of a sub-sample of the objects in a low-frequency selected sample of radio sources in the North Ecliptic Cap (NEC) were obtained on the Nordic Optical Telescope (NOT) in July 1995 and May 1996 (Table 1). The sub-sample consisted of all but one (missed out at random) of the nine extended (radio size $\theta_r > 1''$) $0.5 < z < 0.82$ radio galaxies in a sample based on that of Lacy et al. (1993), with a few additions and deletions made to make the sample complete to a flux density of 0.5 Jy at 151 MHz (the “7C-III” sample; Lacy et al. 1998a). Details of the properties of the sample are given in Table 2. The 1995 July observations were made with the BROCAM camera with a TEK 1024 square CCD and a $0'.176 \text{ pixel}^{-1}$ scale. Those in 1996 May were made with the HIRAC camera, a 2048 square Loral CCD and a $0'.108 \text{ pixel}^{-1}$ scale. Images were made in either R or I , with $0.5 < z < 0.6$ objects in R and $0.6 < z < 0.82$ in I , sampling the rest frame SED at about 450 nm , just above the 4000 \AA break. The images are shown in Fig. 1.

2.2 Spectroscopy

Optical spectra of most of the objects in the 7C-III sample were obtained with the ISIS spectrograph on the William Herschel Telescope (WHT) on 1995 July 28 - August 1. Both the red and blue arms were used, with a 570 nm dichroic used to split the beams and TEK CCD detectors in both arms. The R300R and R300B gratings were used on the red and blue arms respectively. 7C 1815+6815 was observed on 1993 June 17 with a

Table 3: HST observations of the 3C sample

Name	z	Date	Filter	CCD	t_{exp}
3C 34	0.69	10/06/94	F785LP	WF3	1700
3C 41	0.794	29/07/94	F785LP	WF3	1700
3C 172	0.52	19/04/04	F702W	PC	600
3C 226	0.818	04/05/94	F785LP	WF3	1700
3C 228	0.552	14/03/94	F702W	PC	300
3C 247	0.75	29/03/96	F814W	WF3	2400
3C 265	0.811	29/05/94	F785LP	WF3	1700
3C 277.2	0.766	20/06/96	F814W	WF3	2400
3C 337	0.63	24/08/95	F814W	WF3	1400
3C 340	0.76	25/04/94	F785LP	WF3	1700
3C 441	0.708	30/05/94	F785LP	WF3	1700

similar set-up, but an EEV CCD on the red arm with a 540 nm dichroic. A slit width of $3''$ was used, which gave a velocity resolution of $\approx 1500 \text{ km s}^{-1}$ for an object filling the slit. Full details of the observations and data reduction will be given in Lacy et al. (1998c). Emission line fluxes are listed in Table 2, where the estimated emission line contamination of the optical images is also shown.

2.3 Archival HST data

Data on 11 radio galaxies in the sample of Laing, Riley & Longair (1983; hereafter LRL) in the redshift range $0.5 < z < 0.82$, with $\theta_r > 1''$ and $\text{Dec.} < 60^\circ$ were obtained from the HST archive. This sample is complete within the selection criteria with the following exceptions: 3C225B was excluded from the sample due to an uncertainty in its optical identification, 3C352 was excluded due to the presence of a nearby bright star, and 3C55 was inadvertently missed out due to its redshift in LRL being incorrect. The exclusion of these objects is very unlikely to bias the results in any way. Details of the observations are given in Table 3.

3 THE ALIGNMENT EFFECT IN THE 7C SAMPLE

A visual inspection of the images (Fig. 1) reveals a number of objects in which the optical morphology appears aligned with the radio axis. The morphologies of the aligned material differ: in two cases, the hosts are apparently ellipticals with the major axis within 30 deg. of the radio PA, while others (e.g. 7C 1748+6731 and 7C 1826+6510) have multicomponent morphologies along the radio axis similar to that seen in the high luminosity 3C sources. Some individual cases are discussed in more detail below.

7C 1745+6415 This radio galaxy looks like a smooth elliptical, but in fact about 40 percent of the I -band

Table 1: Observations of the low luminosity sample

Name	R.A. (1950)	Dec. (1950)	NOT imaging date & filter	seeing /arcsec	t_{exp} /min	WHT spectrum date	t_{exp} /min	slit PA
7C 1745+6415	17 45 07.30	+64 15 28.6	23/07/96 <i>I</i>	0.6	40	31/07/95	9	177
7C 1748+6731	17 48 50.70	+67 31 38.8	11/05/97 <i>R</i>	0.8	40	29/07/95	10	0
7C 1755+6830	17 55 54.94	+68 30 55.9	10/05/97 <i>I</i>	0.5	40	31/07/95	5	65
7C 1758+6535	17 58 11.58	+65 35 17.1	24/07/96 <i>I</i>	0.9	40	29/07/95	30	52
7C 1807+6831	18 07 06.05	+68 31 11.5	14/05/97 <i>R</i>	0.7	40	29/07/95	10	60
7C 1807+6841	18 07 47.32	+68 41 20.4	25/07/96 <i>I</i>	0.7	40	28/07/95	26	165
7C 1815+6815	18 15 45.69	+68 17 19.2	24/07/96 <i>I</i>	0.9	40	17/06/93	28	100
7C 1826+6510	18 26 31.31	+65 10 45.5	25/07/97 <i>I</i>	0.8	70	28/07/95	30	123

Note: positions are those of the optical identification, and should be accurate to within ≈ 1 arcsec.

Table 2: Properties of the low luminosity sample

Name	S_{151} /Jy	z	Radio size/arcsec	Emission line	Flux / 10^{-20} Wm^{-2}	percent line contamination	Notes
7C 1745+6415	0.59	0.673	5.6	[OII]372.7 H β [OIII]495.9 [OIII]500.7	80 40 140 400	40	
7C 1748+6731	0.64	0.56	108	[OIII]500.7?	9	< 1	absorption line z
7C 1755+6830	1.52	0.744	8.9	[OII]372.7 [NeIII]386.9 [NeV]342.6?	20 17 20	2	
7C 1758+6535	1.13	0.80	106	[OII]372.7 [NeIII]386.9	18 10	1	
7C 1807+6831	2.12	0.580	29	[OII]372.7 [NeIII]386.9 [OIII]500.7	11 8 22	1	
7C 1807+6841	0.60	0.816	12	[OII]372.7 [NeIII]386.9	52 11	< 1	
7C 1815+6815	1.37	0.794	200	MgII 279.8	20	< 1	plus 4000Å break
7C 1826+6510	1.39	0.646	34			< 1	absorption line z

Notes: in all cases the linewidths were below the instrumental resolution for an object filling the slit ($\approx 1500 \text{ km s}^{-1}$) so have not been listed. The errors on the line fluxes are ≈ 15 per cent, excluding aperture corrections. Percentage emission line contamination is the amount of contamination in the filter of observation from the emission lines listed which fall in the filter bandpass. In a few cases emission lines which fall in the *I*-band are beyond the end of the spectra; in these cases their fluxes have been estimated using the emission line strengths in McCarthy (1993).

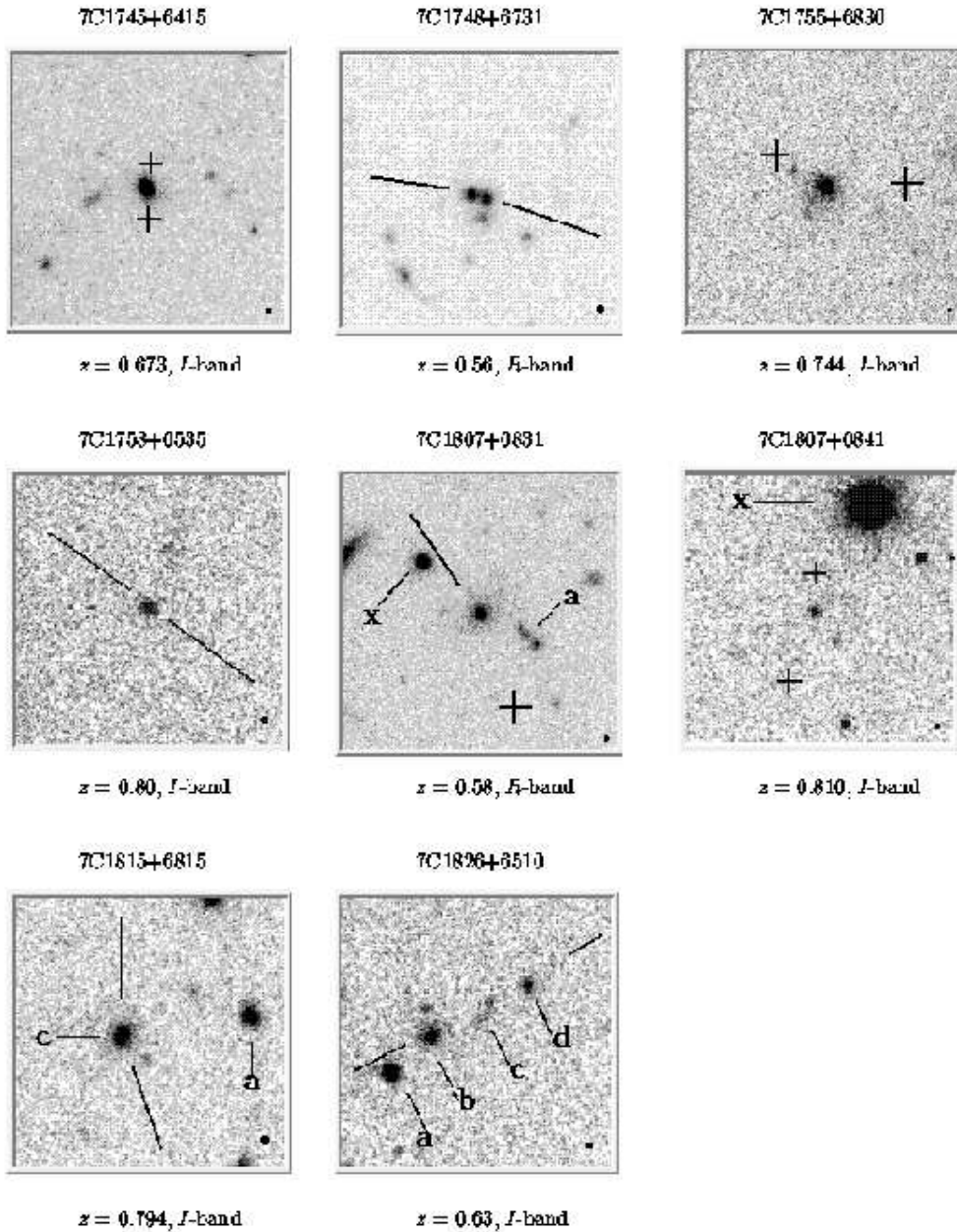


Figure 1: The 7C galaxies analyzed in this paper, with N up, E left. The images are $28''$ square. The black crosses designate the positions of radio hotspots, while the black lines show directions to the hot spots if they fall outside the field. Multiple objects have their individual sub-components labelled. Foreground stars removed from the aperture analysis are labelled with an ‘X’ [apart from 7C1826+6510a which was removed but is labelled ‘a’ for consistency with Lacy et al. (1998b)]. The dot in the SW corner of the image indicates the FWHM of the seeing disc.

light is from emission lines, and consequently the morphology visible in the *I*-band image may be strongly affected by nebular emission. It is therefore not clear in this case whether or not the stellar continuum light is aligned.

7C 1748+6731 This is the most well-aligned object in either sample due to its double structure which is aligned almost perfectly with the radio axis.

7C 1807+6831 The peculiar double component ‘a’ seen to the SW of the host galaxy has the spectrum of a red stellar population consistent with the host redshift. The aligned component has a tentative $H\beta$ emission line

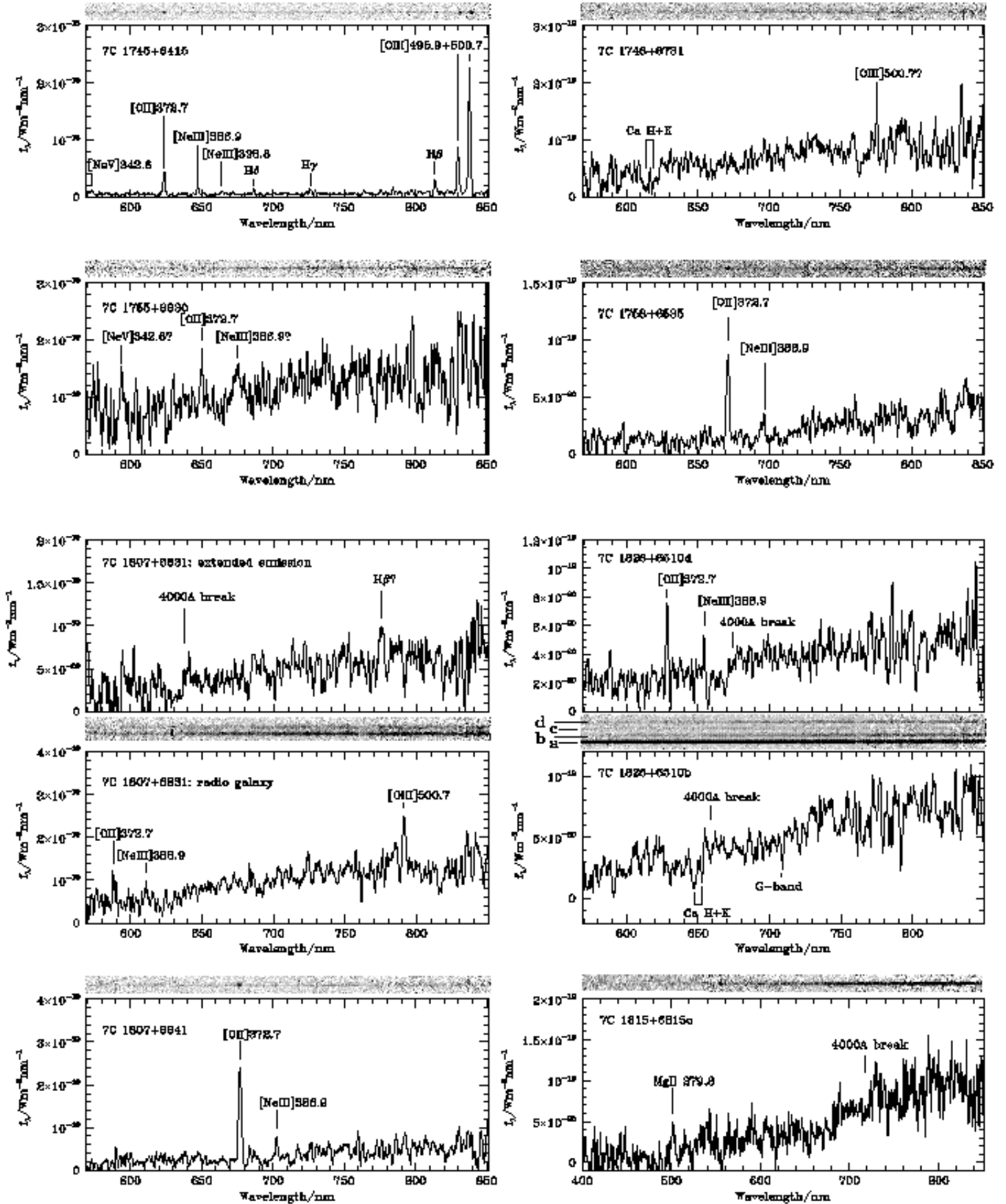


Figure 2: Spectra of the 7C objects. The spectra have been smoothed with a 1.5 nm (5-pixel) box-car filter. Greyscales of the 2D spectra are also shown.

at $z = 0.595$, redshifted by 2800 km s^{-1} relative to the host galaxy. This was checked by cross-correlating the spectra of the host and extended emission (after subtraction of emission lines) with a template spectrum obtained from a high signal-to-noise observation of a low redshift member of the 7C-III sample. This cross-correlation technique yields a redshift of the aligned component of $1300 \pm 700 \text{ km s}^{-1}$ with respect to the host, broadly consistent within the errors.

7C 1815+6815 In Lacy et al. (1993) two possible identifications for this large angular size source were proposed. We have adopted ‘c’ as the identification as it has a weak emission line and is brighter in the H -band (Lacy et al. 1998b). The alternative identification, ‘a’ has a similar stellar spectrum to ‘c’ and is probably in the same group or cluster.

7C 1826+6510 The radio central component detected in an A-array 8 GHz VLA observation (Lacy et al. 1998b) shows that component ‘b’ of Lacy et al. (1998b) is the host galaxy (as claimed by Lacy et al. 1993), although only the aligned component ‘d’ has detected emission lines. Both ‘b’ and ‘d’ have spectra dominated by old stars (Fig. 2). The diffuse component ‘c’ which lies between ‘b’ and ‘d’ also has a red SED, but is too faint for us to be able to tell if it contains stars, or to measure a redshift for. The redshifts of ‘b’ and the stellar component of ‘d’ were determined by the cross-correlation technique described above. We find that ‘b’ has a redshift of 0.646 ± 0.001 and ‘d’ a redshift of 0.685 ± 0.001 (agreeing with the emission line redshift). The velocity difference between these two components is $7100 \pm 400 \text{ km s}^{-1}$, which is high, but not implausible if they are members of a rich cluster. Although clearly well-aligned, ‘d’ lies outside our largest aperture so is excluded from our analysis in the next section. Component ‘a’ is a foreground star and was removed prior to the image analysis.

4 QUANTIFYING THE ALIGNMENT EFFECT

To test whether our apparent detection of an alignment effect in the 7C-III sample is statistically significant, we have attempted to make a quantitative measurement of the “alignment effect” in each galaxy and compared these measurements to those derived for the sample of 3C galaxies in Table 3.

We have used two methods to measure the alignment of the galaxies in these samples: first, a standard moment analysis to derive the difference in the optical position angle from the radio position angle (ΔPA) (Rigler et al. 1992, Dunlop & Peacock 1993, Ridgway & Stockton 1997), and second, a simple derivation of the percentage aligned flux, which should be less susceptible

to skewing by companions and differences in observational resolution. To derive this percentage aligned flux, we have summed the flux within $\pm 45^\circ$ of the lines joining the nucleus to each of the radio hotspots, and subtracted the remaining flux. We exclude from the sums the central portion of each galaxy within the FWHM of the seeing for the ground-based data, and for the archival HST data, we exclude a circular region with a diameter ($0''.5$) comparable to the FWHM of the best seeing ground-based images. This percentage aligned flux value will be positive for images with more flux within the cone of the radio axes than without, and will be negative for objects with more counter-aligned than aligned flux.

To make intercomparisons between objects in this fairly inhomogeneous dataset, we must account both for differences in the depth of the observations and the spread in redshift across the samples. Before analysis, we have therefore resampled the 7C NOT and 3C WFPC2 images to a common pixel scale of $0''.025 \text{ pixel}^{-1}$, and then corrected the surface brightnesses for the differences in cosmological dimming by normalizing to the median redshift of the samples ($z=0.7$) (by assuming that $F_\lambda \propto (1+z)^{-5}$, i.e. that the intrinsic spectra of the galaxies are approximately flat in F_λ at these wavelengths).

A well-known problem with the standard position angle analysis is the subjectivity of choosing the isophotal cutoff level and the aperture within which to calculate the moments (Dunlop & Peacock 1993). Ridgway & Stockton (1997) show that in many cases, however, there is a “dominant” position angle which is approximately constant over a wide range of isophotal cutoffs. The choice of aperture is perhaps more critical, as emission at large radii can easily skew the position angles due to the fact that the PA is determined from the second moment of the intensity distribution. Thus in large apertures, any radio-optical alignments tend to be dominated by the contribution of extended emission and companion galaxies rather than any alignment of the host galaxy itself.

This is borne out in Fig. 3 (a) and (c) where the results of the PA analysis are plotted as a function of isophotal level and aperture size. Provided the isophotes are high enough to be clear of the noise and low enough to include an area of several resolution elements above the isophotal cutoff, the value of the PA in a given small ($\lesssim 3''$) aperture is independent (to about $\pm 10^\circ$) of the exact isophotal level. As discussed above the larger apertures are more sensitive to the isophotal cutoff as they tend to include low surface brightness emission and faint companions which disappear as the isophotal cutoff is raised.

For most of the analysis in this paper, we have chosen a single isophotal cutoff, used for all the images, of $1.0 \times 10^{-23} \text{ W m}^{-2} \text{ nm}^{-1} \text{ pixel}^{-1}$, about 2.5 times the median normalized sky sigma in these frames, for

both the position angle analysis and for the percentage aligned flux analysis. We chose our apertures based on inspection of the behavior of the integrated percentage aligned flux in increasing apertures up to about $10''$ for objects from both samples [e.g. Fig. 3 (b) and (d)]. These indicated that in general there were two spatial regions which tended to contain the major flux contributions: within about $2''$ (~ 15 kpc) and within about $6''$ (~ 50 kpc). These corresponded physically to the approximate isophotal extents of the host galaxies, and to the distance to the nearest few companions respectively. Thus although our choice of apertures is to some extent arbitrary, they correspond to reasonable physical length scales and, as Fig. 3 indicates, varying these apertures by factors of 0.7-1.5 will make little difference to the results. Thus we chose 15 kpc and 50 kpc as the radii of our standard apertures for our analyses.

In all these analyses, we have used as the center the optical center of the identification of the host galaxy. For 7C 1748+6731, we have used the halfway point between the two symmetric optical components (and in this case, also used an exclusion radius of only $0''.05$ for the flux analysis).

A number of objects had foreground stars within the larger aperture which were masked out from the analysis. Those for objects in the 7C sample are marked in Fig. 1. In the 3C sample only 3C 247 had a star removed; the object is to the NE of the radio galaxy and can be recognised from diffraction spikes visible in figure 16(a) of Best et al. (1997b).

For each object in the sample we have calculated the Δ PA and the percentage aligned flux as described above, within these two apertures after making the isophotal cutoff. For many of these objects, which were observed longer or were at lower than median redshift, this standard isophotal cutoff may result in losing obviously well-detected low surface brightness material: for example, large scale extended aligned material in 3C 277.2 falls below this cutoff. This is necessary, of course, to make the comparison on an unbiased basis. We have also calculated the percentage aligned flux in the annulus between 15 kpc and 50 kpc, and we give in Table 4 the results of these analyses for both samples. Also given are the unnormalized aperture magnitudes for the objects.

As a check for the robustness of our result to varying the isophotal levels the PA and percentage flux analysis was repeated, but choosing the isophotal level to be 2.5σ above the background of each individual image. In most cases this made no difference to the PAs and percentage aligned fluxes, and although a couple of individual results changed (for example that for 3C277.2 discussed above) the effect on the statistical analysis discussed in the next section was negligible.

5 RESULTS

The results of our analysis are summarised in Table 4 and Fig. 4. We find that the median percentage aligned flux in the both the 7C and 3C radio sources is positive within the smaller (15 kpc) aperture. The dispersion in the percentage aligned flux is large for both samples, making a meaningful statistical analysis difficult with these small samples. Nevertheless we have attempted to use simple non-parametric statistical methods to estimate the significance of our results.

We give in Figures 4 and 5 histograms of the results of the Δ PA and percentage aligned flux analysis within the 15 and 50 kpc apertures for the 7C and 3C samples. The percentage aligned flux median values given in Table 4 seem to indicate a comparable degree of alignment in the 7C as in the 3C sample, at least at the 15 kpc radius. In the region between 15 kpc and 50 kpc, however, the 3C sample seems more aligned.

To determine whether these results indicate a significant alignment in the 7C and 3C samples, we have made a number of statistical tests, the results of which we give in Table 5. First we determine whether the Δ PA values are consistent with random orientation; a Kolmogorov-Smirnov (K.S.) test of the values versus a uniform distribution (Table 5, lines 1 & 2) shows that at 15 kpc both the 7C and the 3C sample have a probability of less than 1 per cent of being randomly oriented. The same test for the 50 kpc aperture is less conclusive for both samples, as might be expected from an increased slewing of the PA by companion objects, but particularly for the 7C sample (line 3). What about the percentage aligned flux values? We have made a K.S. test to determine whether the 7C and 3C percentage aligned flux distributions differ significantly, and find that in the 15 kpc aperture, there is no significant difference (Table 5, line 5). Within the 50 kpc aperture, and particularly in the 15 – 50 kpc annulus, we find that the probabilities of having such different distributions by chance is significantly reduced (Table 5, lines 6,7,8).

From these tests we can conclude that at least at the 15 kpc scale the 7C sample we have observed seems to exhibit a significant alignment effect. At the larger 50 kpc scale, while the 3C sample continues to show a similar or perhaps increasing amount of aligned flux, the 7C sample is less well aligned.

One potential source of bias in this study is the difference in quasar fraction between the 3C and 7C samples: in the 3C sample of LRL 13/32 of all the radio sources in the redshift range $0.5 \leq z < 0.82$ are quasars, compared to 0/10 objects in the total 7C-III sample. If orientation-based unified schemes of quasars and radio galaxies are true, this may mean that we are missing some 3C objects which are close to the line of sight by selecting only radio galaxies, and hence the mean projected size of the aligned structures in the 3C galaxies will be overestimated. The difference in quasar fraction

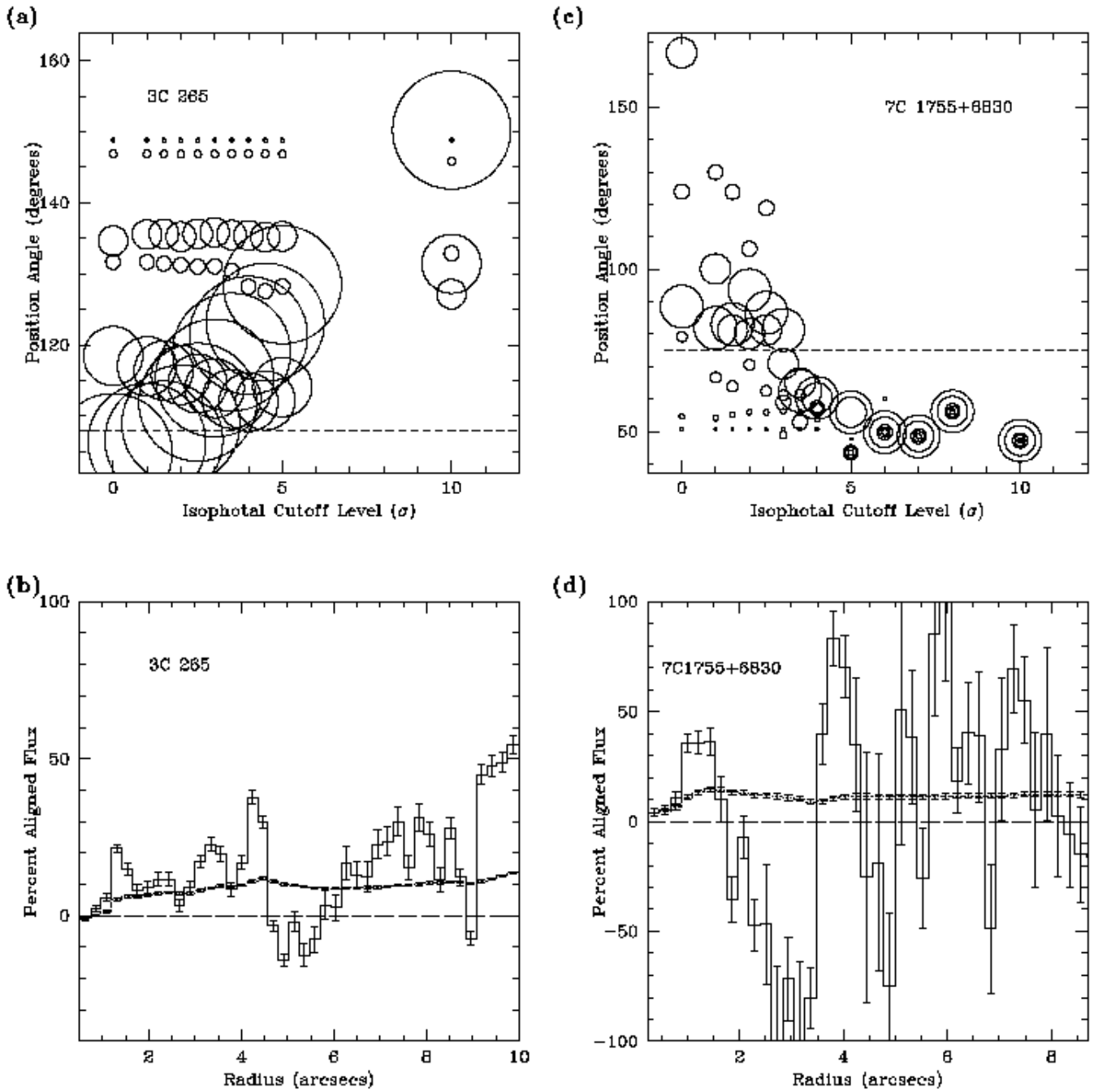


Figure 3: Two examples of results from the analysis methods discussed in this paper. First, for the well-known object 3C265, (a) position angle from a moment analysis versus isophotal level in units of the noise level on the image, σ . This plot shows how the position angle measured in a given aperture varies as the isophotal cutoff is changed. The position angle, measured in apertures of radius $0''.3$, $0''.6$, $1''.2$, $2''.4$, $4''.8$ and $9''.6$ is plotted with circles whose sizes are proportional to the aperture radius. The dashed line is plotted at the PA of the radio axis. In (b) the percentage aligned flux versus aperture radius for 3C265 is plotted. The solid line is the percentage aligned flux within annuli whose radial width is the width of the histogram bar and the dotted line the cumulative percentage aligned flux as a function of radius, obtained by summing the contributions from each annulus within that radius. Second, (c) and (d) are the same plots for the fairly typical 7C radio galaxy 7C 1755+6830(c) and (d). The aperture radii are $0''.54$, $1''.1$, $2''.2$, $3''.0$, $6''.2$ and $8''.6$.

Table 4: Results of alignment analysis

Name	% Aligned Flux (15 kpc)	% Aligned Flux (50 kpc)	% Aligned Flux (15 – 50 kpc)	Δ PA (15 kpc)	Δ PA (50 kpc)	m(AB) (15kpc)	m(AB) (50 kpc)
3C34	4.1 ± 1	-44 ± 1	-68.1 ± 1	20	73	20.0	19.7
3C41	-6.9 ± 1	16 ± 1	96.3 ± 3	88	22	20.9	20.4
3C172	10.6 ± 1	37.2 ± 1	44.8 ± 1	12	23	19.9	18.9
3C226	24.8 ± 1	17.1 ± 1	-8.5 ± 2	2.7	36	20.9	20.3
3C228	-9.9 ± 2	-	-	62	-	19.8	-
3C247	-7.6 ± 1	41.0 ± 1	89.6 ± 1	74	14	20.2	19.1
3C265	7.8 ± 1	15.4 ± 1	23.5 ± 1	19	11	20.1	19.3
3C277.2	22.1 ± 1	3.2 ± 1	-90.0 ± 1	11	75	20.6	20.2
3C337	25.2 ± 1	55.4 ± 1	79.7 ± 1	2.5	10	20.7	20.2
3C340	15.8 ± 1	19.4 ± 1	92.9 ± 7	13	18	21.1	20.8
3C441	18.6 ± 1	27.5 ± 1	33.8 ± 1	17	7	20.8	19.9
Median 3C	11	18	39	17	20	20.6	20.1
7C1745+6415	6.5 ± 1	6.5 ± 1	0 ± 0	35	35	19.7	19.5
7C1748+6731	100 ± 2	100 ± 2	0 ± 0	1.5	1.5	21.1	20.4
7C1755+6830	12.2 ± 1	8.8 ± 1	-6.1 ± 3	22	4	21.0	20.5
7C1758+6535	-3.7 ± 7	-13.4 ± 6	-47 ± 15	2	72	21.4	20.9
7C1807+6831	15.1 ± 1	24.4 ± 1	81 ± 4	11	35	20.6	19.9
7C1807+6841	-9.2 ± 3	-11.5 ± 2	-12.3 ± 2	17	70	21.6	-
7C1815+6815	6.8 ± 2	7.3 ± 2	16.9 ± 10	28	25	20.2	19.7
7C1826+6510	10.3 ± 3	4.5 ± 3	-11.9 ± 6	11	22	20.1	19.5
Median 7C	9	7	-6	14	30	20.8	19.9

(1) The errors given are the statistical errors based on the contribution of sky noise to each sum. (2) The “ 0 ± 0 ” values mean that no flux was left above the isophotal cutoff in those annuli. (3) The 3C 228 image was a very short single PC exposure; only the inner portion was used since all CRs were removed by hand.

may be due to the 7C radio galaxies being members of the class of weak emission line FR II radio galaxies identified by Laing et al. (1994) which have only low optical luminosity quasar nuclei, if any. The quasar fraction in LRL in our chosen redshift range corresponds to an angle to the line of sight of 54° being the angle within which a quasar is seen rather than a radio galaxy. On this basis we might expect the mean projected size of the aligned regions in the 3C sample to be 20 percent larger than that for an isotropic population, but this cannot on its own account for the difference in the scale sizes of the 7C and 3C aligned regions.

5.1 Correlation with overall radio spectral index

Dunlop & Peacock (1993) claim to find a correlation of the fraction of blue light with a combination of radio power and spectral index, which they argue is linked to the aligned light. We find no correlation between aligned flux and rest-frame spectral index measured at 1 GHz in either the 3C or 7C samples, though our samples are somewhat smaller. The lack of any correlation would suggest that the blue light and the aligned light were not simply related: this certainly seems to be the case for the red aligned components discussed in Section 6.4.

5.2 Correlation with radio source size

Best et al. (1996) note a tendency for small $z \sim 1$ radio sources to have very well-aligned, knotty structures, whereas the larger sources often have bimodal, generally less well-aligned structures. We see no tendency in either the 3C or the 7C samples for either the difference in position angle or the aligned flux to correlate with size either at 15 or 50 kpc, although we note that our samples are of both lower mean radio luminosity and lower mean redshift than the Best et al. (1996) objects.

We also checked the extent to which the two samples are similar in terms of properties other than radio luminosity. The spectral index and physical size distributions of the two samples were compared using the K.S. test which showed that the distributions of these quantities are very similar; the probability of the null hypothesis that both are drawn from the same distribution is more than 40 per cent using a two-sided test. Similarly the magnitudes within 15 and 50 kpc are consistent with being the same to 30 per cent on a two-sided test.

6 DISCUSSION

6.1 The comparative strengths and scales of the alignments

Though the results of Section 5 are admittedly based on small samples and are not of great statistical signif-

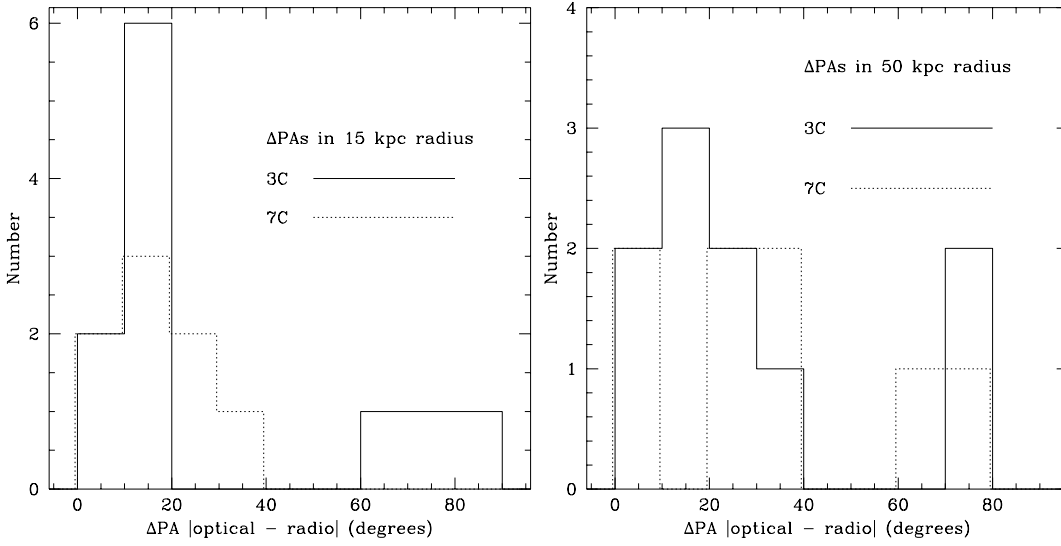


Figure 4: Left: Δ PAs (difference between the optical and radio axes) for the 3C and 7C galaxies within the 15 kpc aperture. Right: Δ PAs for the two samples within the 50 kpc aperture.

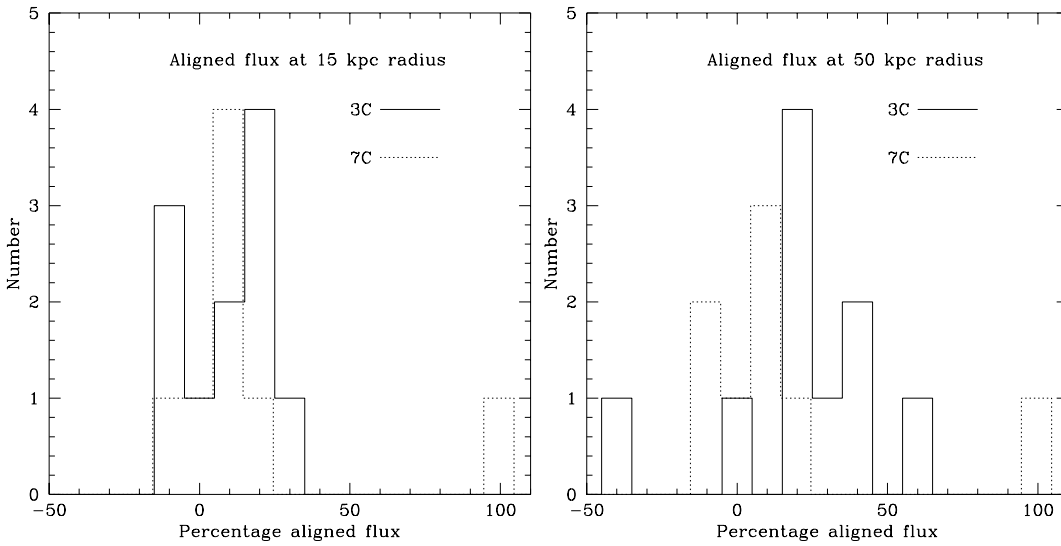


Figure 5: Left: Aligned flux percentage for the 3C and 7C galaxies within the 15 kpc aperture. Right: Aligned flux percentages for the two samples within the 50 kpc aperture.

Table 5: Summary of results of statistical tests

Number	Distributions tested	Type of Test	Result	Probability
1	7C Δ PA (15 kpc) vs. uniform	K.S. (One-sided)	D = 0.617	0.002
2	3C Δ PA (15 kpc) vs. uniform	K.S. (One-sided)	D = 0.505	0.004
3	7C Δ PA (50 kpc) vs. uniform	K.S. (One-sided)	D = 0.361	0.193
4	3C Δ PA (50 kpc) vs. uniform	K.S. (One-sided)	D = 0.444	0.026
5	% Align. Flux (15 kpc): 7C vs. 3C	K.S. (Two-sided)	D = 0.330	0.573
6	% Align. Flux (50 kpc): 7C vs. 3C	K.S. (Two-sided)	D = 0.550	0.095
7	% Align. Flux (15 – 50 kpc): 7C vs. 3C	K.S. (Two-sided)	D = 0.575	0.070
8	% Align. Flux (15 – 50 kpc): 7C vs. 3C	K.S. (One-sided)	D = 0.575	0.035

icance, they are quite suggestive. We seem to have significant alignment on a 15 kpc scale in a sample of radio galaxies whose luminosity is ~ 20 times fainter than that of the 3C sample. Of course, even if we are correct in finding almost comparable percentage alignments in the 7C sample and the 3C sample at ~ 15 kpc, this does not necessarily translate into ascribing the same alignment mechanism to the two samples. An important difference seems to be in the scale of the aligned material.

We have shown that in this sample, the 3C objects are aligned over a large range in scales, whereas in the 7C samples the alignments seem mostly to disappear between 15 and 50 kpc. In the extensively studied $z \sim 1$ 3C galaxies, of which these are probably a reasonably typical subset (though at slightly lower z), it is known that there is a variety of causes for the alignment effect, some of which would work fairly well at large scales, such as scattering. Further evidence for a large-scale aligned component in the 3C radio galaxies is that we find on average twice as much flux above the isophotal cutoff in the 3C as in the 7C in the 15 – 50 kpc annulus, albeit with great dispersion (although we note that the difference in the median magnitudes at 15 and 50kpc is similar in the two samples, suggesting it is relatively compact material in the 3C objects which dominates the large-scale alignments).

Though we do not have in our 3C sample any obvious examples in which the very small scale, “jet path” aligned morphology (e.g 3C 324) dominates, a very small scale alignment mechanism may still be contributing, but is swamped by emission from the more dominant elliptical host. We can probably assume that in this 3C sample the same wide range of mechanisms determined in the $z \sim 1$ samples are contributing, and some of these mechanisms are obviously effective at scales of ~ 50 kpc.

One possibility is that there may simply be less material at larger scales in the 7C environments to be aligned or to act as a scattering medium. An argument against this is the lack of any correlation observed between radio luminosity and galaxy cluster environment at $z \sim 0.5$ (Hill & Lilly 1991). [Our NOT data will eventually be used to quantify the environments of the 7C galaxies directly (Wold, Lacy & Lilje 1998).]

Why, then, are the galaxies in this 7C sample

aligned? We have no information, of course, at the very small ($0''.1$) scale at which some 3C objects show alignment, and our result, though reasonably good statistically, is based on a few objects. Furthermore, these objects themselves show significant variation in the type of aligned morphology. So it is difficult to tell what the likely mechanisms are, and why they do not seem to be operating at ~ 50 kpc scales. Nevertheless, we discuss some possibilities below.

6.2 Mechanisms for alignments at low radio luminosities

Two of the most common alignment mechanisms known to operate in the 3C sample are scattering and nebular continuum emission. Both of these should scale approximately as the emission line strengths, which are found to scale with the radio luminosity to about the 6/7 power (Rawlings & Saunders 1991; Willott et al. 1998). We should therefore expect contributions from scattering and nebular continuum emission to be about a factor of 15 less in the 7C sample than in the 3C sample; were the percentage alignments this much diminished they would have been undetectable. Consistent with this is the fact that some of the 7C radio galaxies have weak or undetectable emission lines, and the quasar fraction is much lower than in 3C (see discussion in Section 5). One would also expect both optical synchrotron and inverse Compton emission (Daly 1992) to scale directly with the radio luminosity.

The probable luminosity dependence of other mechanisms are less clear, but they may scale less severely with radio power. Jet-induced star formation, if it occurs, may even be favoured in lower luminosity sources where the bulk kinetic energy carried by the radio jet is lower. Simulations of shocks propagating into cool clouds have been carried out by a number of groups. Stone & Norman (1992) and Klein, McKee & Colella (1994) have looked at the purely hydrodynamic effects, and show that shock waves with velocities appropriate to supernovae (and therefore probably to most radio-jet induced shocks too) lead to an adiabatic equation of state in the shocked clouds. Such clouds are crushed and shredded due to hydrodynamic instabilities. Mac Low et al. (1994), however, include the effects of magnetic

fields, and find that an equipartition magnetic field may be able to stabilise the clouds against shredding. Foster & Boss (1996) include self-gravity in their simulations, and find that shocks can promote cloud collapse if the shocked gas remains isothermal [typically the case for slow ($< 100 \text{ km s}^{-1}$) shocks], but that adiabatic shocks still lead to cloud shredding. As jet speeds are probably relativistic in FRII radio sources with similar radio luminosities to the 7C sources discussed here (Hardcastle et al. 1998), it certainly seems unlikely that the strong shocks associated with the radio source, for example the bow shock, can lead to star formation. Other, weaker shocks associated with, for example, backflow or the sideways expansion of the lobe, may be more successful, however, particularly on smaller scales within the host galaxy where the densities are high enough that some shocks may be close to isothermal. On the basis of these arguments it seems unlikely that a strong radio jet will be any more successful at forming stars than a weaker one.

The “selection bias” effect of Eales (1992) should also operate effectively in the 7C sample. The strength of the effect in a sample with a narrow redshift range is dependent on the luminosity function at the mean redshift of the sample. Fig. 6 shows the predicted radio – optical position angle distribution for a variety of flux limits at $z = 0.65$, using the Dunlop & Peacock (1990) luminosity-density evolution model. This shows that the 7C sample is sufficiently above the break in the luminosity function that there is very little diminution of this effect in the 7C sample relative to the 3C.

In at least one case (7C 1748+6731) the observed alignment may be due to a dust disk whose axis aligns with the radio jet axis. Aligned dust disk axes are reported to be fairly common in the $z < 0.5$ 3C radio galaxies of the HST snapshot survey (de Koff et al. 1995), and in other HST data on nearby radio galaxies (van Dokkum & Franx 1995). They are thus a viable candidate for producing the 15-kpc scale alignments in the 7C sample. Only one of the 7C (and none of the 3C) sample, however, show evidence for dust lanes, though more may become apparent in the 7C sample at higher resolution.

6.3 Alignments at low redshifts

Studies of radio-optical alignments in low radio-luminosity radio galaxies have, with one or two exceptions, so far been restricted to low redshifts ($z < 0.5$), due to the lack of suitable radio source samples selected at fainter flux levels than 3C. A few individual cases of alignments have been found, but no systematic survey has been fully written up in the literature, although Dey & van Breugel (1993) report finding aligned UV emission in about 30 per cent of nearby ($0.08 < z < 0.2$) powerful radio galaxies. Since the pool of potential sources is very large, and only “interesting”

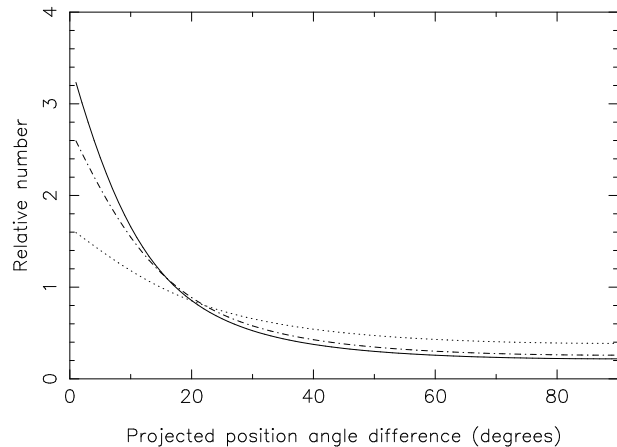


Figure 6: The expected distributions in position angle for $z = 0.65$ radio sources in the model of Eales (1992) as a function of sample flux limit, assuming an ellipticity of 0.33 in the density distribution. Solid curve: 3C ($S_{151} \geq 12 \text{ Jy}$), dot-dash curve: the 7C sample discussed in this paper ($S_{151} \geq 0.5 \text{ Jy}$), dotted curve: a lower flux sample illustrating the fall off in this effect as the luminosity of the radio sources approaches the break in the luminosity function ($S_{151} \geq 0.1 \text{ Jy}$). Although we have only plotted these curves for one value of the ellipticity, changing the ellipticity does not significantly affect the luminosity dependence of this effect.

cases have been published, it is hard to assess whether the low redshift cases are merely coincidences or not, and hard to determine whether there is real evolution between $z \sim 0$ and $z \sim 0.65$.

One systematic survey that has been made is the HST snapshot survey. Objects in the same luminosity range as the 7C objects are in the redshift range $0.1 \lesssim z \lesssim 0.3$ (Fig. 8). In Fig. 7 we plot the difference between the radio and optical position angles for 3C objects in this redshift range, as tabulated by de Koff et al. (1998). Although the isophotal limits and the rest-frame wavelength of observations are somewhat different, both sets of images are taken above the 4000\AA break, so the underlying stellar population might be expected to dominate in both samples. Although there may be a weak alignment trend (note, for example, the lack of objects in the $80\text{--}90^\circ$ bin), there is clearly no strong alignment effect in this sample.

The individual low redshift cases of radio-optical alignment that have been published actually span a wide range in radio luminosity. To illustrate this, in Fig. 8 we plot some of the better known low luminosity aligned objects, together with our 3C and 7C samples, on the radio-luminosity redshift plane.

Perhaps the most famous example of an FRI radio source with aligned emission is PKS0123-016A, where the blue peculiar galaxy known as Minkowski’s object is seen apparently interacting with the radio jet (van Breugel et al. 1985). The FRI radio sources in A1795

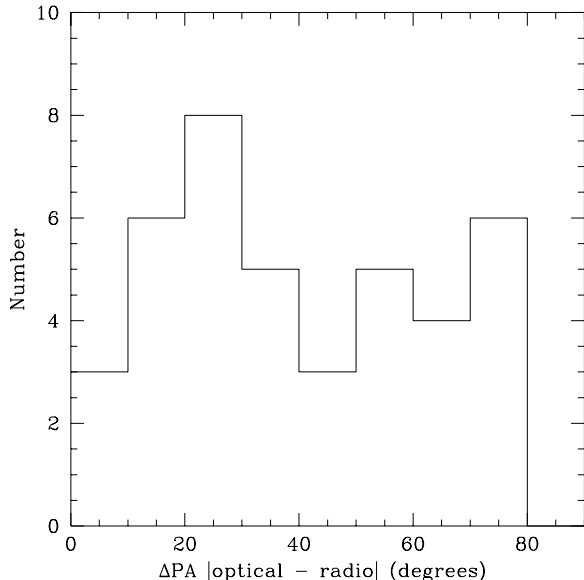


Figure 7: The distribution of ΔPA for the 40 objects in the HST snapshot survey with $0.1 < z < 0.3$ (de Koff et al. 1998).

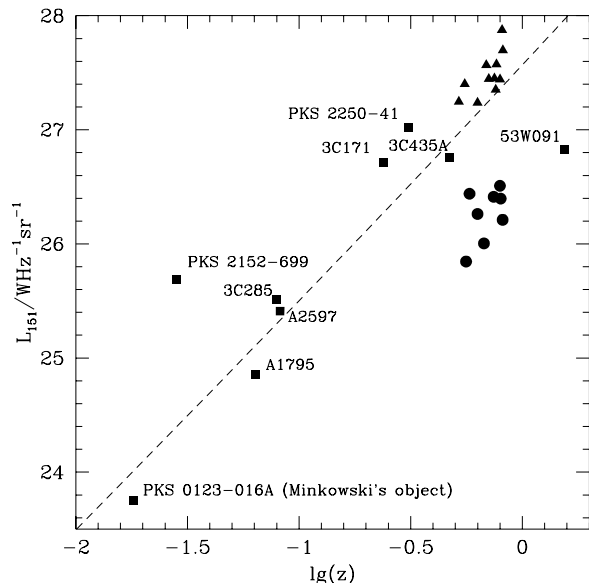


Figure 8: A radio luminosity - redshift plane diagram illustrating the range in radio luminosities of the radio - optical alignments discussed in this paper. Solid triangles: the 3C sample of Table 3, solid circles: the 7C sample of Table 1. Solid squares represent other sources from the literature. The dashed line corresponds to the flux limit of the 3CR from which the HST snapshot survey objects were selected.

and A2597 have been studied by McNamara and collaborators. They find excess blue light in the host galaxies which appears to trace the radio lobes but which is unpolarised (McNamara et al. 1997; McNamara et al. 1996; Sarazin et al. 1995; McNamara & O'Connell 1993). All these cases of the alignment effect in FRI radio galaxies seem best explained via jet-induced star formation. Indeed, as discussed in Section 6.2, jet-induced star formation may be easier in sources with lower jet velocities.

3C285 is an FRII radio source close to the FRI/FRII boundary which has a blue aligned component projected ≈ 70 kpc from the nucleus which van Breugel & Dey (1993) ascribe to jet-induced star formation (the host galaxy itself is not aligned). PKS 2152-699, another low luminosity FRII has an aligned blue knot whose light is polarised at 90° to the radio axis, which suggests that scattered light from the nucleus is responsible. (di Serego Alighieri 1989; Fosbury et al. 1998). Both these objects are a little less radio-luminous than the 7C objects.

Aligned emission has also been seen in more powerful FRII radio sources, notably 3C171 (where nebular continuum seems to be responsible; Clark et al. 1998), PKS 2250-41 (Clark et al. 1997) and 3C435A (Rocca-Volmerange et al. 1994). The latter two cases are discussed below.

6.4 Red companion alignments

Two of the objects in the 7C sample, 7C1807+6831 and 7C1826+6510 have aligned components with red stellar populations. Furthermore, the morphology of these components is peculiar, with both having fainter aligned material strung out along the line joining them to the radio source host galaxy. There are a number of other similar red aligned objects in the literature, and they provide some of the most puzzling manifestations of the alignment effect. Examples include 3C34 (Best et al. 1997a), 3C114 (Dunlop & Peacock 1993; Leyshon & Eales 1998) 3C212 (the SE component; Ridgway & Stockton 1997; Stockton & Ridgway 1998), 53W091 (Spinrad et al. 1997), 3C356 (whichever of 'a' or 'b' is the true host; Lacy & Rawlings 1994; Cimatti et al. 1997), 3C435A (Rocca-Volmerange et al. 1994), PKS 2250-41 (Clark et al. 1997) and 3C441 (Lacy et al. 1998). These objects can be divided into two classes, those where the companion is just beyond a radio hotspot (3C212, 53W091, 3C435A, 3C441, PKS2250-41) and those where it is within a lobe (3C34, 3C114, 3C356, 7C 1807+6831, 7C1826+6510).

Those with optical components close to hotspots can probably be explained in terms of a radio jet colliding with a galaxy in the same group or cluster as the host. The increase in external density will raise the ram pressure in the head of the source, enhancing the syn-

chrotron emissivity and thereby pushing the source into a flux-limited sample.

Those with optical components in the lobe are more puzzling [except perhaps for 3C114 which is polarized in K -band; Leyshon & Eales (1998)]. Chance, or unusually well-aligned manifestations of the selection effect of Eales (1992) could explain their presence, but if so their often peculiar morphologies (e.g. 3C34 and the two 7C objects in this paper) remain a puzzle. A possible, but perhaps unlikely explanation, given the discussion in Section 6.2, is that jet-induced star formation could occur with an IMF weighted heavily towards massive stars and lead to an aligned component dominated by a red stellar population in $\sim 10^7$ yr (Lacy & Rawlings 1994; Best et al. 1997a).

6.5 Implications for photometry of radio galaxy hosts

Could a component of aligned light on large scales whose luminosity is proportional to that of the AGN affect near-infrared studies of $z \sim 1$ radio galaxies? Roche, Eales & Rawlings (1998) find that the K -band sizes and magnitudes of $z \sim 1$ radio source hosts differ significantly between the 3C and 6C samples, which are only a factor of four different in radio flux limit, and Best et al. (1998) claim to find extended haloes around their HST images of 3C radio galaxies which they suggest may be cD galaxy haloes. However, there is a significant K -band alignment effect seen in 3C radio galaxies (Rigler et al. 1992; Dunlop & Peacock 1993; Ridgway & Stockton 1997) which is not present in the 6C objects (Eales et al. (1997). Also, the 6C and 7C samples follow similar $K - z$ relations despite the factor of five between the 6C and 7C flux limits (Rawlings et al. 1997), again consistent with the idea that the 3C galaxies are significantly contaminated by emission which scales with the power of the AGN. Estimates of the amount of AGN light contributing in the K -band fall short of the amount required to explain the difference between the 3C and 6C/7C $K - z$ relations, however. Rigler et al. (1992) argue that the aligned component seen in the 3C galaxies contributes only ≈ 10 per cent of the total near-infrared emission, and Simpson, Rawlings & Lacy (1998) show that the effect of the reddened quasar nucleus is only about a 15 per cent correction to the mean magnitude at $z \approx 1$. This would predict that 3C galaxies should be about 0.25 mag brighter than 6C ones, compared to the 0.59 mag difference between the 3C and 6C mean galaxy magnitudes (in 63.9 kpc apertures) measured by Eales et al. (1997). As yet there is also no direct evidence that the larger scale-sizes of the 3C radio galaxies are connected to the aligned light. Nevertheless, the difference in the mean magnitudes of 3C and 6C galaxies after allowing for the contributions of aligned light and reddened quasar nuclei is sufficiently small that high spatial resolution infrared imaging and

spectroscopy will probably be required to finally resolve this issue.

7 CONCLUSIONS

A possible explanation for the scale difference we see in the alignments of the 3C and 7C radio galaxies is that the alignment mechanisms that operate at the large scales in the 3C are the most luminosity dependent. Both scattering and nebular continuum could be argued to fall into this category provided enough material exists at large radius to intercept light from the hidden quasar.

The small-scale alignment that we seem to see in the 7C sample indicates that some less luminosity-dependent alignment mechanism, effective at moderately small scales, may be contributing to the “alignment effect” that we see in radio sources. That the 3C alignments extend to larger scales could mean that this less-luminosity dependent alignment mechanism is swamped by other effects, such as scattering, in the more powerful radio sources. Possible candidates for this small-scale alignment mechanism include jet-induced star formation, dust discs with axes parallel to the radio axis, and the selection effect of Eales (1992) (assuming the PA of the host galaxy is parallel to that of the major axis of the density distribution on the scale size of the radio source).

In addition, there are two cases of more extended aligned light in the 7C sample. In both cases old stellar populations are seen in the brightest aligned components. They may be present due to selection effects, but jet-induced star formation with a peculiar IMF cannot be ruled out, and may explain the unusual morphology of the aligned light.

The detection of alignment in the $z \sim 0.7$ 7C sample also suggests the alignment effect has a component which is truly due to cosmic evolution in the host galaxies of radio sources, and not just due to the increase in radio luminosity with redshift present in flux-limited samples. Systematic observations of low redshift 3C radio galaxies in directly comparable wavebands are required to confirm this, however.

The presence of an alignment mechanism (or mechanisms) which scales only weakly with radio luminosity may imply that even a fairly weak radio AGN can influence the morphology and perhaps even stellar content of its host. This would have implications for attempts to search for old elliptical galaxies at high redshifts through spectroscopy of faint radio sources (e.g. Dunlop et al. 1996). On the other hand, if dust lanes or selection effects are responsible, then such galaxies may be ideal for studying the oldest stellar populations at high redshift. It is thus important to establish what this small-scale alignment mechanism is, and it is clear that higher resolution observations of a fainter radio

source sample than 3C would be of great help in this respect.

ACKNOWLEDGMENTS

We thank Christian Kaiser for helpful comments on the manuscript and the staff at the NOT and WHT for their help with the observations. SER is supported by a PPARC PDRA grant. The NOT is operated jointly by Denmark, Finland, Iceland, Norway and Sweden, and the WHT by the Isaac Newton Group both on the Island of La Palma in the Spanish Observatorio del Roque de los Muchachos of the Instituto de Astrofísica de Canarias. This paper was also partly based on observations made with the NASA/ESA Hubble Space Telescope, obtained from the data archive at the Space Telescope Science Institute. STScI is operated by the Association of Universities for Research in Astronomy, Inc. under the NASA contract NAS 5-26555.

REFERENCES

- Baum S.A., Heckman T., 1989, *ApJ*, 336, 702
- Best P.N., Longair M.S., Röttgering H.J.A., 1996, *MNRAS*, 280, L9
- Best P.N., Longair M.S., Röttgering H.J.A., 1997a, *MNRAS*, 286, 785
- Best P.N., Longair, M.S., Röttgering H.J.A., 1997b, *MNRAS*, 292, 758
- Best P.N., Longair M.S., Röttgering, H.J.A., 1998, *MNRAS*, 295, 549
- Chambers K.C., Miley G., van Breugel, W. 1987, *Nature*, 329, 609
- Chambers K.C., Miley G., van Breugel W. 1990, *ApJ*, 363, 21
- Cimatti A., Dey A., van Breugel W., Antonucci R., Spinrad H., 1996, *ApJ*, 145, 156
- Cimatti A., Dey A., van Breugel W., Hurt T., Antonucci R., 1997, *ApJ*, 476, 677
- Clark N.E., Axon D.J., Tadhunter C.N., Robinson A., O'Brien P., 1998, *ApJ*, 494, 546
- Clark N.E., Tadhunter C.N., Morganti R., Killeen N.E.B., Fosbury R.A.E., Hook R.N., Siebert J., Shaw M.A., 1997, *MNRAS*, 286, 558
- Daly R.A., 1992, *ApJ*, 386, L9
- de Koff S., Baum S.A., Sparks W.B., Biretta J.A., Golombek D., Macchetto F., McCarthy P.J., Miley G.K., 1995, *Bull. A.A.S.*, 187.1202
- de Koff S., Baum S.A., Sparks W.B., Biretta J.A., Golombek D., Macchetto F., McCarthy P.J., Miley G.K., 1996, *ApJS*, 107, 621
- Dey A., Spinrad H., 1996, *ApJ*, 459, 133
- Dey A., van Breugel W., 1993, *Bull. A.A.S.*, 182.0421
- Dey, A., van Breugel, W., Vacca, W., Antonucci, R. 1997, *ApJ*, 490, 698
- Dickinson M., Dey A., Spinrad H., 1995, in, Hippelein H., Meisenheimer K., Röser H.-J., eds, "Galaxies in the Young Universe". Springer-Verlag, Berlin p. 164
- Dickson R., Tadhunter C., Shaw M., Clark N., Morganti R., 1995, *MNRAS*, 273, L29
- di Serego Alighieri S., Fosbury R.A.E., Tadhunter C.N., Quinn P.J., 1989, *Nat*, 341, 307
- Dunlop J.S., Peacock J.A., 1990, *MNRAS*, 247, 19
- Dunlop J.S., Peacock J.A., 1993, *MNRAS*, 263, 936
- Dunlop J., Peacock J., Spinrad H., Dey A., Jimenez R., Stern D., Windhorst R., 1996, *Nat*, 381, 581
- Eales, S.A. 1992, *ApJ*, 397, 49
- Eales S.A., Rawlings S., Law-Green D., Cotter G., Lacy M., 1997, *MNRAS*, 291, 593
- Fosbury R.A.E., Morganti R., Wilson W., Ekers R.D., di Serego Alighieri S., Tadhunter C.N., 1998, *MNRAS*, 296, 701
- Foster P.N., Boss A.P., 1996, *ApJ*, 468, 784
- Hardcastle M.J., Alexander P., Pooley G.G., Riley J.M., 1998, preprint: astro-ph/9811203
- Hill G.J., Lilly S.J., 1991, *ApJ*, 367, 1
- Klein R.I., McKee C.F., Colella P., 1994, *ApJ*, 420, 213
- Lacy M., Hill G.J., Kaiser M.E., Rawlings S., 1993, *MNRAS*, 263, 707
- Lacy M., Blundell K.M., Hill G.J., Kaiser M.E., Rawlings S., 1998a, in preparation
- Lacy M., Kaiser M.E., Hill G.J., Rawlings S., 1998b, submitted
- Lacy M., Rawlings S., Hill G.J., Bunker A., Ridgway S.E., Stern D., 1998c, in preparation
- Lacy M., Rawlings S., Blundell K.M., Ridgway S.E., 1998, *MNRAS*, 298, 966
- Lacy M., Rawlings S., 1994, *MNRAS*, 270, 431
- Laing R.A., Jenkins C.R., Wall J.V., Unger S.W., 1994, in, Bicknell G.V., Dopita M.A., Quinn P.J., eds, *ASP Conf. Ser.* 54, *The Physics of Active Galaxies*. Astronomical Society of the Pacific, p. 201
- Laing R.A., Riley J.M., Longair M.S., 1983, *MNRAS*, 204, 151 (LRL)
- Leyshon G., Eales S.A., 1998, *MNRAS*, 295, 10
- Longair M.S., Best P.N., Röttgering H.J.A., 1995, *MNRAS*, 275, L47
- McCarthy P.J., van Breugel W., Spinrad H., Djorgovski S., 1987, *ApJ*, 321, L29
- McCarthy P.J., 1993, *ARA&A*, 31, 639
- Mac Low M.-M., McKee C.F., Klein R., Stone J.M., Norman M.L., 1994, *ApJ*, 433, 757
- McNamara B.R., Jannuzi B.T., Sarazin C.L., Wise M., Elston R., 1997, *Bull. A.A.S.*, 191.106.07
- McNamara B.R., Jannuzi B.T., Elston R., Sarazin C.L., Wise M., 1996, *ApJ*, 469, 66
- McNamara B.R., O'Connell, 1993, *AJ*, 105, 417
- Martel A.R., Sparks W.B., Macchetto D., Biretta J.A., Baum S.A., Golombek D., McCarthy P.J., de Koff S., Miley G.K., 1998, *ApJ*, 496, 203
- Rawlings S., Saunders R., 1991, 349, 148
- Rawling S., Saunders R., Eales S.A., Mackay C.D., 1989, 240, 701
- Rawlings S., Blundell K.M., Lacy M., Willott C.J., Eales S.A., in, Bremer M., ed, *Cosmology with the New Radio Surveys*, in press
- Ridgway S.E., Stockton, A., 1997, *AJ*, 114, 511
- Rigler M.A., Stockton A., Lilly S.J., Hammer F., Le Fèvre O., 1992, *ApJ*, 385, 61
- Rocca-Volmerange B., Adam G., Ferruit P., Bacon R., 1994, *A&A*, 292, 20
- Roche N., Eales S., Rawlings S., 1998, *MNRAS*, 297, 405
- Sarazin C.L., Burns J.O., Roettiger K., McNamara B.R., 1995, *ApJ*, 447, 559
- Serjeant S., Rawlings S., Maddox S.J., Baker J.C., Clements D., Lacy M., Lilje P.B., 1998, *MNRAS*, 294, 494
- Simpson C.J., Rawlings S., Lacy M., 1998, *MNRAS*, submitted
- Spinrad H., Dey A., Stern D., Dunlop J., Peacock J., Jimenez R., Windhorst R., 1997, *ApJ*, 484, 581
- Stockton A., Ridgway S.E., Kellogg M., 1996, *AJ*, 112, 902
- Stockton A., Ridgway S.E., 1998, *AJ*, 115, 1340
- Stone J.M., Norman M.L., 1992, *ApJ*, 390, L17
- van Breugel W.J.M., Filippenko A.V., Heckman T.M., Miley G.K., 1985, *ApJ*, 293, 83

- van Breugel W.J.M., Dey A., 1993, ApJ, 414, 563
van Dokkum P.G., Franx M., 1995, AJ, 110, 1027
Willott C.J., Rawlings S., Blundell K.M., Lacy M., 1998, MN-
RAS, in press
Wold M., Lacy M., Lilje P.B., 1998, in preparation.